



This is a repository copy of *Oscillating coal and biomass flames: A spectral and digital imaging approach for air and oxyfuel conditions*.

White Rose Research Online URL for this paper:

<http://eprints.whiterose.ac.uk/127626/>

Version: Accepted Version

Article:

Farias Moguel, O., Szuhanszki, J., Clements, A.G. orcid.org/0000-0003-3778-2248 et al. (3 more authors) (2018) Oscillating coal and biomass flames: A spectral and digital imaging approach for air and oxyfuel conditions. *Fuel Processing Technology*, 173. pp. 243-252. ISSN 0378-3820

<https://doi.org/10.1016/j.fuproc.2018.02.002>

Article available under the terms of the CC-BY-NC-ND licence
(<https://creativecommons.org/licenses/by-nc-nd/4.0/>).

Reuse

This article is distributed under the terms of the Creative Commons Attribution-NonCommercial-NoDerivs (CC BY-NC-ND) licence. This licence only allows you to download this work and share it with others as long as you credit the authors, but you can't change the article in any way or use it commercially. More information and the full terms of the licence here: <https://creativecommons.org/licenses/>

Takedown

If you consider content in White Rose Research Online to be in breach of UK law, please notify us by emailing eprints@whiterose.ac.uk including the URL of the record and the reason for the withdrawal request.

OSCILLATING COAL AND BIOMASS FLAMES: A SPECTRAL AND DIGITAL IMAGING APPROACH FOR AIR AND OXYFUEL CONDITIONS

*Farias Moguel, O.^a, Szuhánszki, J.^a, Clements, A.G.^a, Ingham, D.B.^a, Ma, L.^a, Pourkashanian, M.^a

^aEnergy 2050, Faculty of Engineering,
The University of Sheffield, Sheffield, UK, S10 2JT

ABSTRACT

The transient nature of a flame can be quantified by performing spectral and oscillatory analysis of its parameters, such as the flame's luminance and temperature. This paper presents an assessment of the effect of an oxyfuel environment on the combustion of two different solid fuels, a high volatile bituminous coal and a white wood biomass, in a 250 kW_{th} pilot-scale combustion test facility. A digital flame monitoring system was fitted to the experimental furnace, and was used to record high speed videos of the flame. Transient signals for both digital luminance and temperature were obtained after the instantaneous frames were extracted from the original videos. Spectral analysis was performed over the transient signal in order to analyse the temporal coherence of the flame through a weighted oscillation frequency value. An additional parameter, the oscillation index, which accounts for the amplitude of the oscillation of the flame, was computed to complement the information recovered from the flame. The oscillation trends obtained from these experiments assess the dynamic response of the flame to different combustion environments within the furnace. In general, it was found that oxyfuel flames showed a discernible temporal repeatability and a lower magnitude of the oscillation of their flame parameters, and therefore are registered as being more stable than their counterpart under air combustion conditions. In addition, the biomass flames exhibit less sensitivity to the oxyfuel combustion environment than what was found with coal, which may allow future oxy-biomass regimes to operate under a much wider envelop of firing conditions.

1. Introduction

The combustion of fossil fuels, such as coal, currently meets the majority of the global energy demand [1]. However due to the significant proportion of the worldwide greenhouse gas emission directly associated to its usage, further improvements to the efficiency and control of the combustion process are needed, as well as the implementation of less carbon intensive fuels under the same infrastructure[2], [3]. In addition, novel technologies such as carbon capture and storage (CCS) have been developed in an effort to achieve a low-carbon process that maintains the benefits of fossil fuel usage [4], [5]. Oxyfuel combustion is a very promising CCS technology, where the air in the combustion process is replaced with a mixture of recycled flue gas and oxygen producing a high CO₂ outflow that can be effectively processed for long term storage or utilisation. The adjustment of the combustion environment within the boiler resulting from the high CO₂ concentration will modify the flame characteristics from a fundamental level, and therefore it is important to properly evaluate the changes of the flame that occur with different flue gas recycle schemes [6]–[9].

A solid-fuel flame is often characterised by its physical parameters, such as the flame size, shape, luminance and temperature. The oscillatory behaviour of a flame can be quantified by spectral and amplitude analysis for the instantaneous variations of the previously referred flame parameters [10].

A flame is usually considered to be stable across its parameters if the quantified variations of them does not induce flame blow off or flash back into the burner [11]–[13].

Digital imaging systems provide a non-intrusive method to quantify the flame parameters, and have been widely used through a range of fuels and combustion conditions [14]. The spectral analysis methodology over the flame parameters have been previously applied to both premixed and diffusion gas flames [15], [16]. A similar technique was then adapted for a wider range of fuels, such as heavy-oil [17]. In parallel, a similar approach was used to characterize solid fuel flames, such as pulverised coal under air [18]–[20], and lately under oxy-combustion conditions [21]. In addition, spectral analyses have been successfully used within computational fluid dynamics models to assess the oscillation mechanisms of swirling flows and combustors [22], and their impact on the predicted flame stability [23], [24].

The combustion of biomass, either as a primary fuel or as a part of a fuel blend, has been advised as an effective way to decrease the environmental impact of power generation [25]–[28]. In addition, the association of CCS technologies to biomass combustion (BECCS), if properly managed, offers negative CO₂ emissions to the atmosphere, increasing its relevance as an alternative to decrease the current CO₂ concentration to the pre-industrial levels as prescribed in international climate change agreements [29]–[31]. Flame imaging techniques have been used to assess the stability of the combustion process in terms of its oscillation and the displacement of the ignition point for different biomass fuels on an industrial-scale furnace [32]. Special attention has been given to analyse coal-biomass blends and its impact on the flame stability and to the boiler operational limit through different methodologies, including flame imaging [8], [15], [33]–[35]; however, the research published on the effect of the oxyfuel environment to the biomass combustion has been focused on the ignition temperature and burnout over an entrained flow reactor [36]–[38].

This paper presents the results of an experimental campaign undertaken for coal and biomass under air and oxyfuel conditions on the solid combustion test facility at the UKCCSRC Pilot-scale Advanced Capture Technology (PACT) Core Facilities. A detailed description of the experimental facilities is presented in Section 2. Four different combustion scenarios were tested for each fuel, consisting of an air-fired and three oxyfuel cases with oxygen enrichment levels of 24, 27 and 30-vol% of the combustion gases fed to the furnace. The details of each case are discussed in Section 4. Spectral and oscillation analyses were performed after equally extracted sets of frames consisting of 8000 RGB images; the methodology for this purpose is introduced in Section 3. The results obtained from the experiments are discussed in Section 4. Finally, a summary of the findings and the conclusions of this research are presented in Section 5.

2. Experimental facilities

The experimental campaign was performed at the UKCCSRC Pilot-scale Advanced Capture Technology (PACT) Core Facilities, located in South Yorkshire, UK. The PACT 250 kW air/oxyfuel Combustion Test Facility (CTF) consists of a down-fired, cylindrical furnace, which is 4 m in height with a 0.9 m internal diameter. A frontal view of the furnace is shown in Figure 1. The furnace is assembled from eight sections, which are 0.5m in height, with each section internally lined with a 0.1 m thick layer of refractory material. The test rig is designed to be capable of allocating both intrusive and non-intrusive probes by providing each section with a wide range of measuring ports. The furnace is operated under a low induced draft by coupling a centrifugal fan to the exhaust pipe.



Figure 1. Digital representation of the combustion test rig and the digital imaging system.

The furnace was fitted with two different scaled versions of commercially available low NO_x burners, one for each type of fuel. A 250 kW_{th} burner manufactured by Doosan Babcock was used for the coal combustion cases, while a 250 kW_{th} burner by General Electric was installed for the biomass combustion tests. Both burners were designed to produce a swirled flame by directing the oxidant fluid and the fuel through an arrangement of three concentric annular sections, each of them containing a fixed-blade array. The fuel is carried by a small portion of the oxidant through the inner annulus, referred as the primary channel, while the remainder of the oxidiser is introduced to the furnace through the secondary and tertiary annuli. The different internal configuration of the burners, from which each company is proprietary, allows the rig operator to adjust the ratio of oxidant flowing through the secondary and tertiary as well as the angular momentum as required.

3. Methodology

An image based system was employed for the quantification of the flame stability. The system comprises a water-cooled optical probe fitted with a wide angle lens used to guide the perceived light into the complementary metal-oxide-semiconductor (CMOS) sensor of an industrial type RGB camera. The CMOS sensor is embedded into an integrated circuit and coupled to a personal computer installed with a dedicated software that is then used to record videos of the flame. The system has the capability to modify the sample speed from which a series of still RGB images, or frames, are captured and merged into a video. The maximum recording speed of the optical array is 265 frames per second with a resolution of 320×256 pixels.

The series of still RGB images are extracted from the recorded videos. Each frame consists of a matrix array of size M×N×3 where M and N are the number of pixels in width and height of the image and 3 is the number of colour channels from which the light spectrum is divided and recorded by the camera sensor. The colour channels obtained from the image are red, green and blue. Each channel matrix consists of evenly quantized 24-bit values for each location (pixel) within the region captured by the camera sensor. Three different approaches were used for the flame stability assessment using the same set of frames. The first approach is based on the brightness of the flame,

represented as the digital luminance value, which is largely associated with the motion of combusting char particles [32]. The second approach employs the temperature value computed by the two colour method [40], accounting for all of the volume contained within the flame region, including the possible volatile and char combustion oscillatory effects, as well as those of their derived highly radiant products, such as soot particles. Finally, an overall oscillation index is computed after the whole light spectrum captured by the camera and the magnitude of the variations in the colour hue, intensity and saturation from the images [41]. Spectral analysis for the first two methods is performed in order to assess the repeatability of their correspondent parameters, accounting for the flame temporal dynamics, while the last method blends the transient variations and the magnitude of its parameters into a single comprehensive term that reflects the severity of the oscillatory behaviour of the flame.

3.1. Digital luminance

The digital luminance, Y , for each pixel in the matrix array was calculated using the weighting expression:

$$Y = \alpha_1 R + \alpha_2 G + \alpha_3 B \quad (1)$$

where R , G and B are the quantized values for each pixel in the primary colour channels, red, green and blue respectively, from which the light spectrum was captured by the installed camera. The values for the weighting constants are set up as $\alpha_1 = 0.2989$, $\alpha_2 = 0.587$ and $\alpha_3 = 0.114$ [42].

3.2. Temperature

The temperature estimation of the flame was performed using the relationship between captured colours proposed by Lu et al. [40]. In this study the red-green relationship is employed:

$$T = \frac{(C_2) \left(\frac{1}{\lambda_G} - \frac{1}{\lambda_R} \right)}{\ln \frac{R}{G} + \ln S + \ln \left(\frac{\lambda_R}{\lambda_G} \right)^5} \quad (2)$$

where C_2 is the second Planck's constant, 1.4387×10^{-2} mK; λ_R is the peak wavelength of the red spectrum, 615 nm; λ_G is the peak wavelength of the green spectrum, 540 nm; R is the value for each pixel in the red channel; G is the value for each pixel in the green channel and S is the apparatus factor, obtained experimentally [40], [43] and is given by,

$$S = (0.3653) \left(\frac{R}{G} \right)^2 - (1.669) \left(\frac{R}{G} \right) + 3.392 \quad (3)$$

3.3. Power spectral density and the characteristic oscillatory frequency

Arithmetic mean values of the pixels for each approach are computed, assigning a single value to every frame. The transient variation of the mean values for the computed parameters is then converted into a signal.

The dynamic nature of the flame is then characterized by constructing the frequency spectrum after each parameter signal. The power spectral density for every frequency band is derived from:

$$P(f) = \frac{1}{n_s} (FFT_{n_s}(f))^2 \quad (4)$$

where $P(f)$ is the power spectral density value, $FFT_{n_s}(f)$ is the fast Fourier transform of the n_s sampled points parameter signal. The value of $P(f)$ at $f = 0$ Hz, commonly known as the DC component, is not taken into account as it is not associated to the dynamic nature of the flame [44].

Even though the frequency spectrum reveals the fluctuating behaviour and temporal coherence of the flame in terms of a relevant parameter, it is important to note that the overall oscillation of the flame comprises an intertwined accord of all of the frequencies from which the whole spectrum was divided. A weighted-average value for the contribution of each frequency band has been calculated as the characteristic oscillatory frequency for each parameter using the following expression:

$$F = \frac{\sum_{i=1}^{n_f} [P_i \cdot f_i]}{\sum_{i=1}^{n_f} P_i} \quad (5)$$

where F is the characteristic oscillatory frequency, P_i and f_i are, respectively, the power spectral density and the frequency of the i th band within the constructed spectrum, and n_f is the number of bands from which the constructed spectrum was divided. The characteristic frequency F , as a weighted value, represents the repeatability of a flame parameter oscillation in the temporal domain.

3.4. The oscillation index

An overall oscillation index of the flame, with a range between 0 and 1, is introduced after the pixel values are obtained from the recovered frames. The RGB values are converted into the hue, saturation and intensity (HSI) of the image in order to dissociate the intensity variations from the colours. The HSI pixel values for each image are calculated as follows [45]:

$$H = \cos^{-1} \left(\frac{\frac{1}{2}[(R - G) + (R - B)]}{[(R - G)^2 + (R - B)(G - B)]^{1/2}} \right) / 360^\circ \quad \text{For } B \leq G \quad (6a)$$

$$H = 1 - \cos^{-1} \left(\frac{\frac{1}{2}[(R - G) + (R - B)]}{[(R - G)^2 + (R - B)(G - B)]^{1/2}} \right) / 360^\circ \quad \text{For } B > G \quad (6b)$$

$$S = 1 - \frac{3}{R + G + B} \cdot [\min(R, G, B)] \quad (7)$$

$$I = \frac{R + G + B}{3} \quad (8)$$

The mean and contrast values, M_k and C_k respectively, of the pixel matrix are computed for each HSI colour component as

$$M_k = \frac{1}{M \times N} \sum_{i=0}^{M-1} \sum_{j=0}^{N-1} U_k(i, j) \quad (9)$$

$$C_k = \left(\frac{1}{M \times N} \sum_{i=0}^{M-1} \sum_{j=0}^{N-1} (U_k(i, j) - M_k)^2 \right)^{1/2} \quad (10)$$

where $k = H, S$ or I and $U_k(i, j)$ is the i th- j th pixel element of the $M \times N$ frame. An additional parameter, A_I , corresponding to the relative flame area is obtained after a background removal operation. For this purpose, each frame was converted into a binary image using a threshold estimated from the grey-level histogram from which each pixel $U_I(i, j)$ [46]:

$$U_I(i, j) \begin{cases} 1, & \text{if } > \text{threshold} \\ 0, & \text{if } \leq \text{threshold} \end{cases} \quad (11)$$

The relative area of the flame is then defined as:

$$A_I = \frac{1}{M \times N} \sum_{i=0}^{M-1} \sum_{j=0}^{N-1} U_I(i, j) \quad (12)$$

The seven parameters obtained after the transient array of HSI images are then merged into a single value, the oscillation index, by using the corresponding standard deviation and maximum dynamic values:

$$\delta = \prod_{i=1}^7 \left(\frac{\phi(X_i) - \sigma_{X_i}}{\phi(X_i)} \right)^{w_i} \quad (13)$$

where $X_i \in \{M_H, M_S, M_I, C_H, C_S, C_I, A_I\}$ and σ_{X_i} correspond to the standard deviation of the flame parameter X_i ; $\phi(X_i)$ is the dynamic range of the measured signal for each computed parameter of the flame, where $\phi(X_i) = 0.5$ for M_H, M_S, M_I, A_I and $\phi(X_i) = 0.25$ for C_H, C_S, C_I . In addition, w_i represents a weighting factor for each of the computed parameters; w_i values are set to represent the importance of one parameter against each other, for this particular study $w_i = 2$ for all parameters, thus acknowledging them as equally important [45].

4. Experimental results and discussion

The experimental campaign was carried out on the PACT 250 kW air/oxy-fired CTF, at the UKCCSRC PACT Core Facilities located in South Yorkshire, UK. A batch of ‘El Cerrejón’, a high volatile bituminous South American coal, was used alongside milled white wood biomass from the United States. The calorific values and composition properties of both fuels are shown in Table 1.

'El Cerrejón' coal				White wood biomass			
Ultimate analysis (%, DAF)		Proximate analysis (% as received)		Ultimate analysis (%, DAF)		Proximate analysis (% as received)	
Sulphur	0.52	Moisture	7.63	Sulphur	<0.02	Moisture	6.69
Carbon	80.92	Ash	2.90	Carbon	48.44	Ash	0.70
Hydrogen	5.12	Volatile matter	35.50	Hydrogen	6.34	Volatile matter	78.10
Nitrogen	1.65	Fixed carbon (by diff.)	53.98	Nitrogen	0.15	Fixed carbon (by diff.)	14.51
Oxygen (by diff.)	11.79			Oxygen (by diff.)	37.69		
Gross calorific value [MJ/kg]		29.61		Gross calorific value [kJ/kg]		19.41	
Net calorific value [MJ/kg]		28.41		Net calorific value [kJ/kg]		18.10	

Table 1. Properties of the fuels used on the experimental campaigns.

Four cases were recorded for each fuel, consisting of one air-fired and three oxyfuel cases with overall O₂ concentrations of 24, 27 and 30-vol % supplied by an O₂/CO₂ mixing-skid. The O₂ concentration in the fuel-carrier flow channel (primary) was retained at 21 %vol for all oxyfuel cases in order to ensure safe operation of the rig. Thus the target concentration for each case was achieved through mixing a higher O₂ concentration stream from the secondary and tertiary channels. Due to the discrepancies in the internal design of each burner, the ratio of oxidant mixture conducted through the primary channel was set up as 20% of the overall fluid flow entering the furnace for coal combustion tests and as 18% for the biomass; the remaining flow is then split into secondary and tertiary streams in the wind box of the burner. Several preliminary tests were carried in order to adjust the aerodynamics of the flame across the different combustion scenarios proposed in order to reduce NO formation whilst maintaining an optimum fuel burnout. The thermal load was set for all the experimental campaigns as 200 kW_{th} for coal and 200 kW_{th} for the biomass cases. The operating conditions of the rig under air and oxyfuel cases are summarised in Table 2.

Coal combustion campaign				Biomass combustion campaign					
Case	Primary flow		Secondary-Tertiary flow		Case	Primary flow		Secondary-Tertiary flow	
	Air [l/min]	Air [l/min]	Air [l/min]	Air [l/min]		Air [l/min]	Air [l/min]	Air [l/min]	Air [l/min]
Air	825		3250		Air	676		3076.6	
Oxy24		O ₂ [l/min]	CO ₂ [l/min]	O ₂ [l/min]	O ₂ [l/min]	CO ₂ [l/min]	O ₂ [l/min]	CO ₂ [l/min]	
Oxy24	138	523	657	1992	Oxy24	119	449	641	1951
Oxy27	124	464	674	1677	Oxy27	107	399	654	1648
Oxy30	111	419	685	1428	Oxy30	94	360	666	1398

Table 2. Operating conditions used in the experiments.

The flame imaging system was paired to the furnace using a port located in the top section of the furnace in order to get a direct view of the flame. All of the remaining ports were sealed in order to prevent air leaking into the furnace. In order to reduce the risk of missing data due to system saturation, a recording speed of 200 fps was used for the experimental campaigns. The exposure for all of the recorded cases was set at 1.5 ms, and both the focus and aperture of the sensor were manually tuned prior to the campaigns and were retained throughout the whole study.

Two different regions of interest were used to compute the stability of the flame, the first corresponds to the allocation of the maximum captured length of the flame, and the second region is focused on the domain close to the burner, often referred to as the root region, in which due to a larger amount of volatiles, flow mixing and emissions formation phenomena are dominant [44]. A set of 8000 images of 320×256 pixels were extracted from 40 s videos for all of the cases. The captured frames were post processed using a computational algorithm coded into Matlab R2015a, to extract the relevant digital luminance and temperature signals. A preliminary assessment showed that the oscillation in the temperature signal was highly damped by the hot walls of the furnace captured as background. In order to mitigate this impact the global threshold algorithm proposed by Otsu [46] was implemented to select the pixels that will be used for the temperature calculation, thus isolating the flame region from the background. A second set of images for the air, Oxy27 and Oxy30 cases was used in order to assess the repeatability of the study, a comparison of the results showed differences below 1% of the captured spectrum for all cases and regions analysed; additionally, the oscillation index exhibited an average difference of 4.4% for all cases.

4.1. Coal combustion spectral analysis

4.1.1. Full flame region

Each of the extracted frames from the video were trimmed into a 190×235 pixel area. The smaller images were then used to construct both the luminance and temperature signals. A single frame for each coal combustion case is shown in Figure 2, alongside their corresponding luminance and temperature processed values. The normalized frequency spectrums for both the luminance and temperature approaches are displayed in Figure 3. It has been previously reported that oscillation frequencies higher than 10 Hz are generally associated to the combustion of gas-phase volatile species, while frequency values around 1 Hz can be related to the slower rate for char combustion [47]. The referred spectrums were computed up to the maximum Nyquist frequency of 100 Hz, however no significant values of the power spectral density, $P(f)$, were observed beyond 10 Hz; therefore plots of the frequency spectrums are shown up to that value throughout this study.

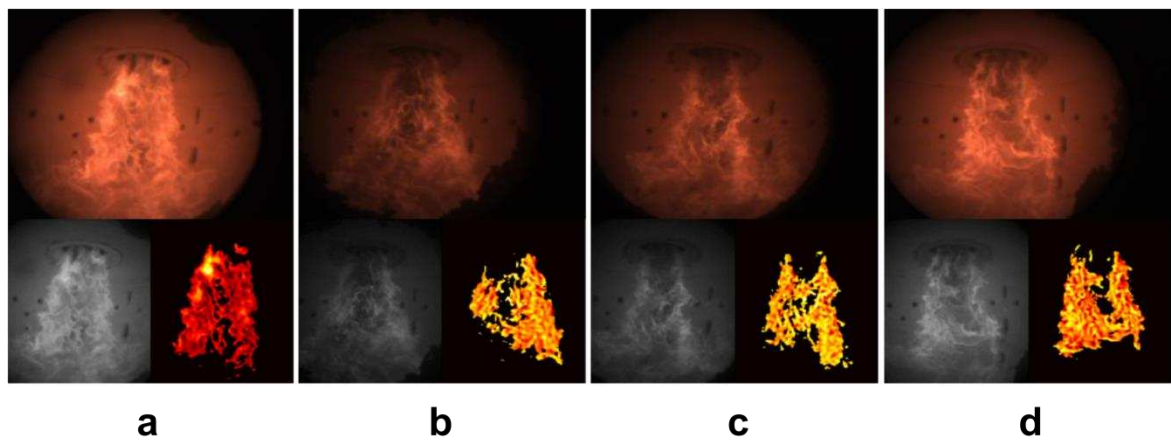


Figure 2. Original and processed frames from the coal combustion studies using full flame region; a) air-fired, b) Oxy24, c) Oxy27 and d) Oxy30.

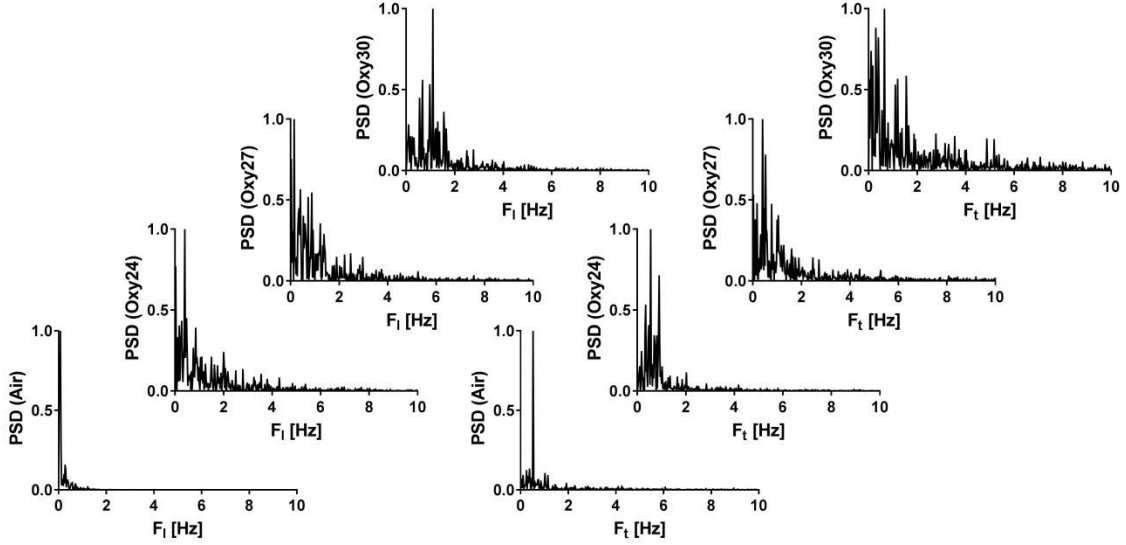


Figure 3. Frequency spectrums constructed for the luminance (left) and temperature (right) approaches for the coal flame.

As it can be observed from Figure 3, the frequency spectrums for the oxyfuel cases are more unsettled in comparison to the air fired cases. Nevertheless, the majority of the relevant frequencies are contained below 4 Hz. The weighted value of the oscillation frequency for the luminance approach, presented in Figure 4, shows a narrow difference, suggesting a similar char burnout rate between all of the cases, with all of the frequencies being between 1.8 and 1.9 Hz. On the other hand, the temperature-based frequencies show a larger oscillation for the Oxy24 and Oxy27 in comparison to the air fired case, with values of 2 and 2.6 times higher, respectively. The trend then shows a sharp decrease for the frequency of the Oxy30 case, dropping to a value of 3.6 Hz, which is closer to the frequency measured for the air case at 2.6 Hz, which could be a possible consequence of the lower diffusivity of oxygen in a CO₂ enriched environment and lower adiabatic flame temperatures [7].

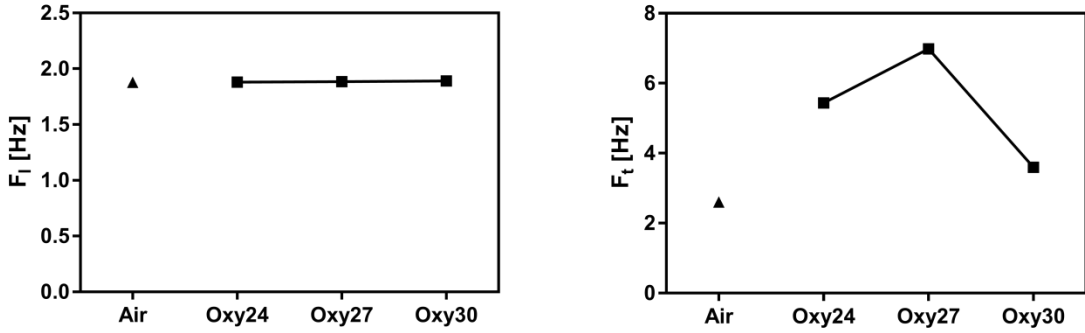


Figure 4. Weighted oscillation frequencies for the luminance (left) and temperature approach for coal combustion.

4.1.2. Root region

A pixel area of 190×100 from the same set of frames used for the previous calculation was used for the root region. The region of interest was carefully positioned within the original frame in order to fully include the burner outlet. The processed luminance and temperature frames are displayed in Figure 5.

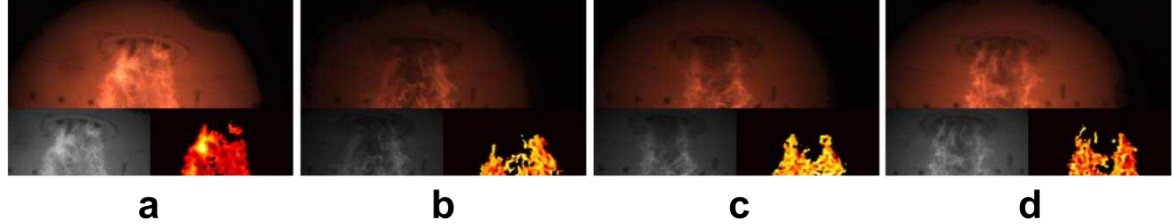


Figure 5. Original and processed frames for the coal combustion studies using root region of the flame; a) air-fired, b) Oxy24, c) Oxy27 and d) Oxy30.

The normalised spectrums for both methodologies, presented in Figure 6, show a similar arrangement to those obtained for the full flame, with the cluster of relevant frequencies concentrated in the low range and with no noticeable values for the power spectral density above the 6 Hz band for the majority of the cases. However, the weighted values for the oscillatory frequencies, Figure 7, are higher in magnitude. The values obtained from the luminance signal were closely grouped between 2.3 and 2.55 Hz, while the weighted values for the temperature approach, as expected for a high volatile content zone, show a bigger difference between the air fired oscillation frequency calculated at 2.2 Hz and the oxyfuel estimations at 9.3, 8.2 and 6.3 Hz for the Oxy24, Oxy27 and Oxy30 scenarios, respectively.

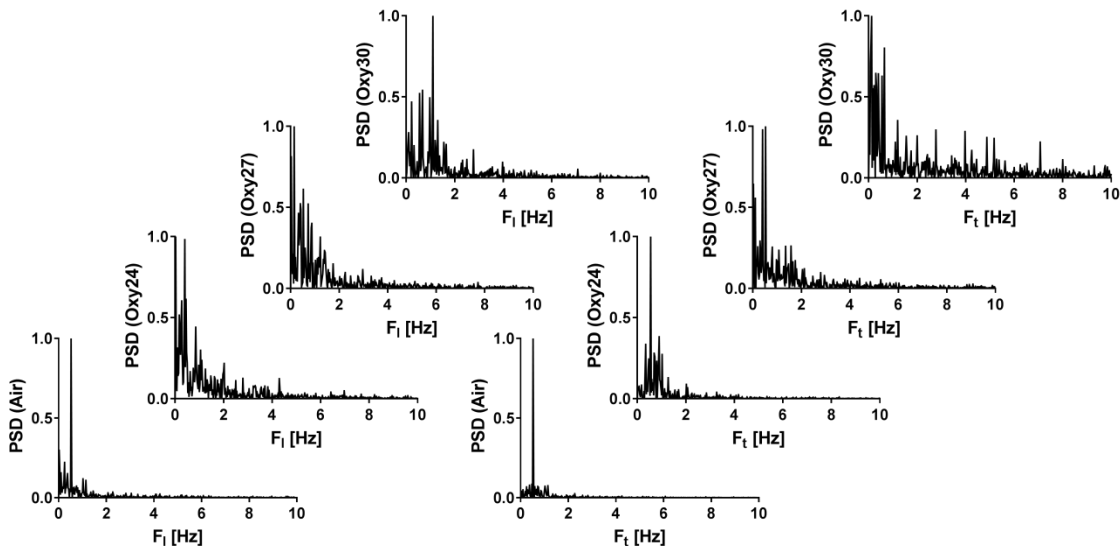


Figure 6. Frequency spectrums computed for the root region of the coal flame using the luminance (left) and temperature (right) approaches.

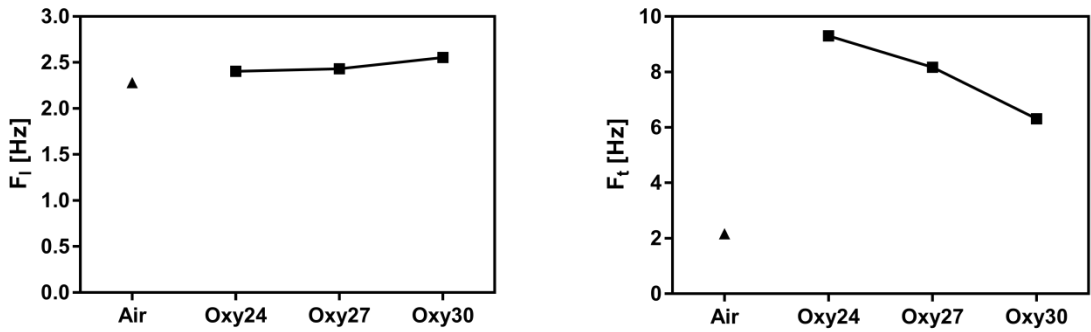


Figure 7. Weighted frequencies after the luminance (left) and temperature (right) oscillations in the root region of the coal flame.

4.2. Biomass combustion spectral analysis

4.2.1. Full flame region

A similar procedure to that applied to the coal combustion cases was carried out for the extracted frames during the biomass combustion campaign. The biomass flame for the Oxy24 case is found to be wider in comparison to the generated flames for all of the other combustion scenarios, nevertheless the same pixel area of 190x235 was retained for the sake of consistency between calculations. A sample image for all the tested conditions besides its corresponding luminance and temperature counterparts are shown in Figure 8.

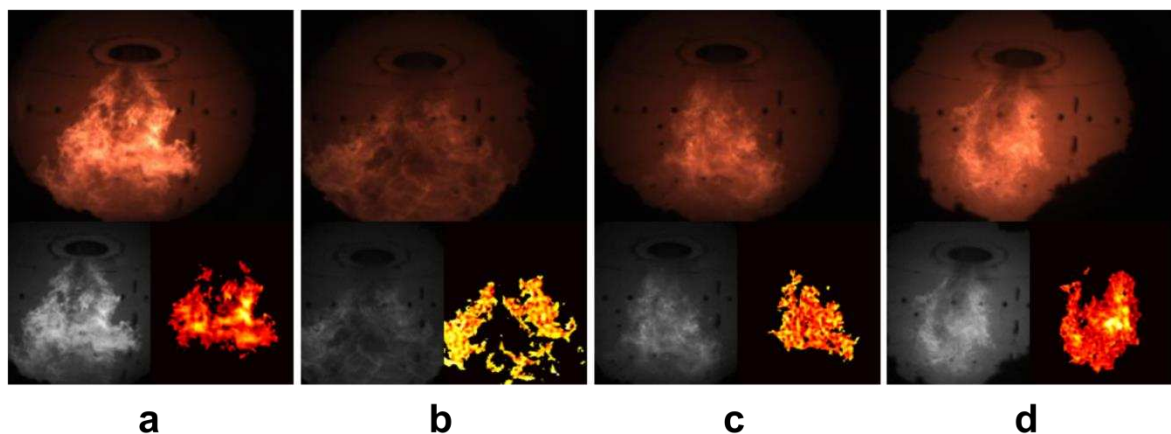


Figure 8. Original and processed frames for the biomass combustion cases using full flame region; a) air-fired, b) Oxy24, c) Oxy27 and d) Oxy30.

The frequency spectrums composed using the luminance and temperature transient signals appear to be sharper in comparison to those obtained from coal flames. Up to three distinctive frequencies can be observed for each case from both the luminance and temperature-based spectrums, Figure 9. Both the air-fired and the oxyfuel cases show a relevant frequency around 1 Hz for the transient luminance analysis. In addition, the air and Oxy27 cases share significant contributions to their oscillatory behaviour from frequency bands at 1.8 and 2.9 Hz. The weighted values for the

luminance-formulated oscillation frequency are arranged between 2.5 and 3 Hz for the air, Oxy24 and Oxy30, with the value for the Oxy27 case being slightly below at 2 Hz which is mainly due to the larger power spectral density value, $P(f)$, for the low range frequencies.

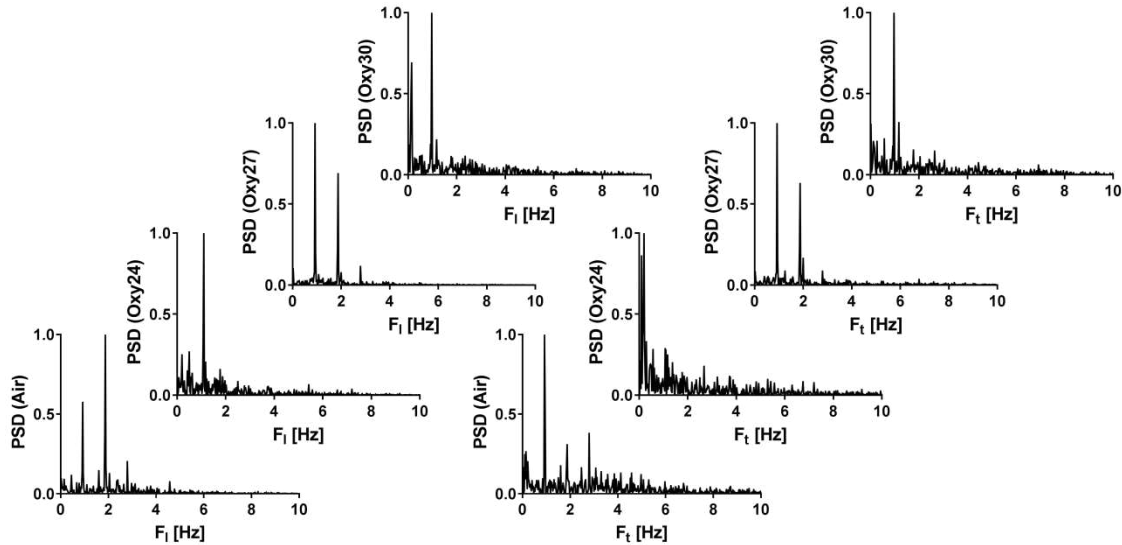


Figure 9. Frequency spectrums constructed for the luminance (left) and temperature (right) approaches after the full region of the biomass flames.

The spectral analysis of the temperature signals show similar results as the luminance study, with the air, Oxy24 and Oxy30 cases exhibiting their most significant frequencies around 1 Hz. In addition, the air and Oxy27 case appear to share a second frequency at 1.9 Hz. In contrast, the spectrum after the temperature signal for the Oxy24 case turned out to be more dispersed across the lower range of frequencies, with a single discernible cluster of frequencies around 0.2 Hz. Likewise, the weighted values, presented in Figure 10, show an oscillation frequency for air and Oxy27 cases of approximately 5.2 Hz, while Oxy30 show a relatively lower frequency at 4.3 Hz. As a result of a more diffuse spectrum, the Oxy24 case generated a higher oscillation frequency of 7 Hz.

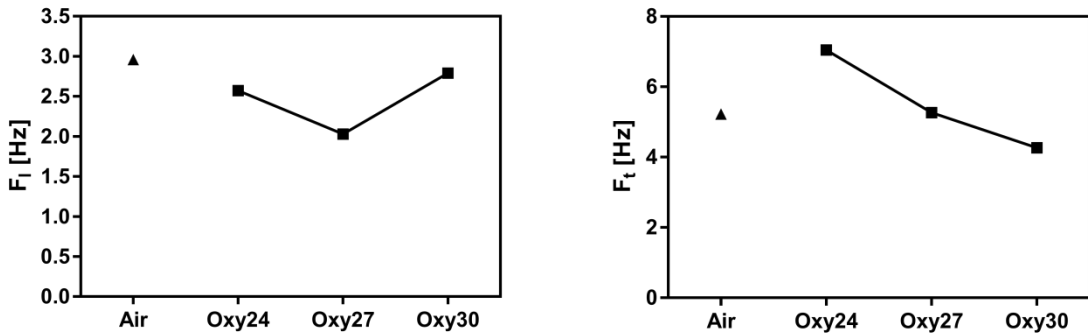


Figure 10. Weighted frequencies for the full region of the biomass flames after the luminance (left) and temperature (right) approaches.

4.2.2. Root region

Following a similar procedure as for the coal combustion cases, a pixel area of 190×100 from the same set of frames used in the previous section was processed in order to generate their corresponding signals for the luminance and temperature parameters in the root region. Single frames are shown in conjunction with their corresponding processed values for both techniques in Figure 11.

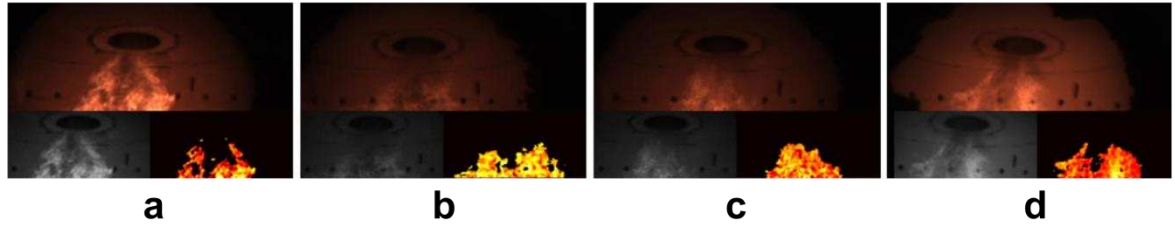


Figure 11. Original and processed frames for the biomass flames using root domain; a) air-fired, b) Oxy24, c) Oxy27 and d) Oxy30.

In all of the cases, in a similar fashion as for the full flame region, a noticeable contribution from the frequencies around 1 Hz is clearly noticed in the spectrum constructed for the luminance signal, displayed in Figure 12. However, an additional frequency was observed in the lower region of the spectrum, which in the case of the Oxy30, test represents the peak value for the power spectral density of the whole spectrum. These low frequencies reside within 0.2 and 0.4 Hz in all cases. The weighted values for the frequencies presented in Figure 13, show that the values obtained using the luminance approach are distributed in pairs, with values for the air and Oxy30 case of 3.1 and 3.2 Hz, and 3.6 and 3.8 Hz for the Oxy27 and Oxy30 cases, respectively.

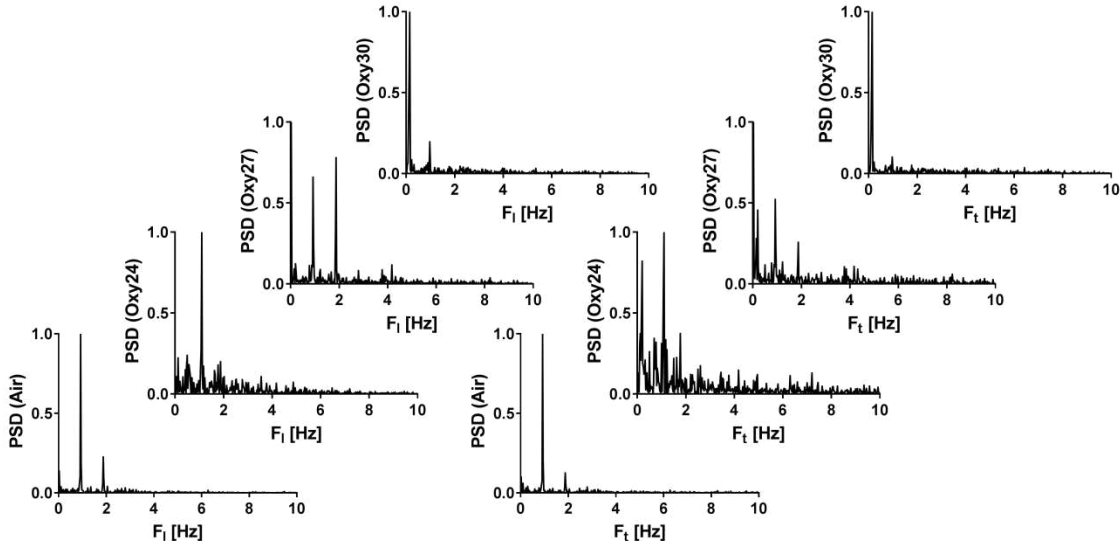


Figure 12. Frequency spectra for the luminance (left) and temperature (right) methodologies computed for the root region of the biomass flames.

The frequency spectrums obtained from the temperature method show that the contribution from each computed band is spread along a much wider range for the Oxy24 and Oxy27 scenarios, while both for air and Oxy30 a single dominant frequency is noticeable. Low value frequencies up to 0.5 Hz, akin to those obtained for the full flame are observed only for the oxyfuel cases. A similar trend for the weighted frequencies to those obtained for the full flame is noticed however their values are narrowly arranged, with air and Oxy30 sharing a value of 5.8 Hz, whereas Oxy24 and Oxy27 cases oscillate at 13 and 13.1 Hz, respectively.

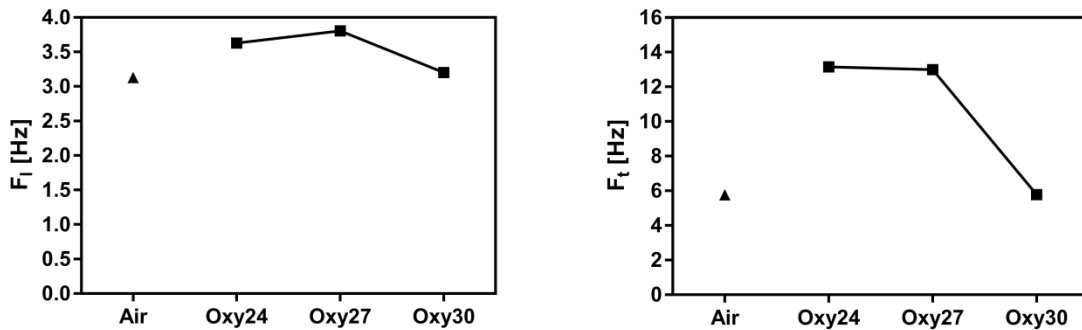


Figure 13. Weighted frequencies for the luminance (left) and temperature (right) approaches on the root region of the flame.

4.3. Oscillation analysis

4.3.1. Full flame region

The oscillation index, δ , was computed after converting the same set of frames used for the spectral analyses to the hue, saturation and intensity (HSI) space. The oscillation index is established as a relationship between the mean value and the standard deviation of the HSI parameters and the area of the flame, thus providing a value to account for the extent of the flame oscillation. By definition, a value of 1 for the oscillation index represents a flame in which all of the measured parameters remain constant through the analysed period, while a value of 0 describes the highest possible oscillation, and can only be obtained if the one of the parameters is ranging between its maximum and minimum values across each sampled image. In consequence, the stability of a flame can be established as directly proportional to the value of its oscillation index.

The trend of the oscillation index for the coal combustion cases, Figure 14, shows higher values for the oxyfuel cases, ranging between 0.75 for Oxy24 and Oxy30, and 0.82 for the Oxy27 case, in comparison to the more unsettled air fired test with a value of 0.66.

Moreover, the oscillation index for the full flames in the biomass combustion campaign, exhibit a higher value for both the lower and higher oxygen enriched scenarios tested; the oscillation index value was 0.78 and 0.83 for the Oxy24 and Oxy27 cases, respectively. In a similar fashion to coal combustion, the air-fired case showed the lowest value of the oscillation index for the biomass campaign at 0.71, while the Oxy27 case generated a value of 0.74. The range of the oscillation index for all of the biomass cases was narrower in comparison to the observed trends in the coal

combustion campaign, therefore the stability of the flame appears to be less affected when switching to the oxyfuel combustion environment for biomass cases.

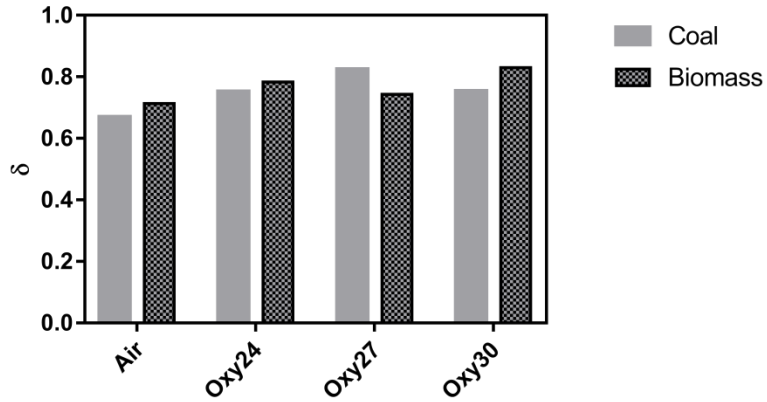


Figure 14. Oscillation index for the full flame region.

4.3.2. Root region

The oscillation index for the root region of both coal and biomass flames, presented in Figure 15, shows that, in agreement with the results for the full flame domain, the oxyfuel cases appear to oscillate less than the air combustion scenario. The root region of the coal flames showed that the oscillation index value for the air fired case was 0.65, while the values for the oxyfuel conditions increased in direct proportion to the oxygen concentration from 0.74 for the Oxy24 case, 0.80 and 0.81 for the Oxy27 and Oxy30 cases, respectively. In addition, the biomass combustion shows the same trend to that acquired using the full flame region; however, the flame root of the Oxy27 case shows the lowest oscillation index value at 0.68, whereas for Oxy24 and Oxy30 it is 0.78 and 0.85, respectively; the oscillation index for the air-fired case was acquired at 0.73. A direct comparison with the values obtained for the full flame region shows that the relative trends of the index appears to be insensitive to the sampled area.

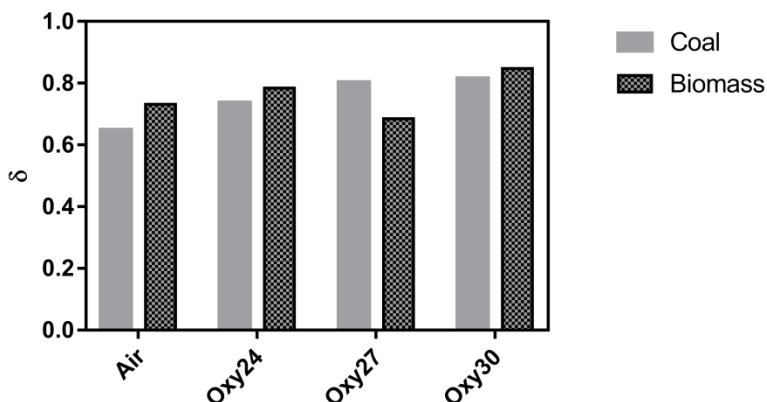


Figure 15. Oscillation index for the flame root region.

5. Conclusions

An assessment of the flames produced by coal and biomass was made based on a digital imaging system. A spectral analysis of the transient digital luminance and the temperature variations calculated from the still images of the flame were used as an indicator of the flame oscillatory behaviour and their repeatability over time. A third parameter, in the form of the overall oscillation index, was introduced. The oscillation index is computed after the fluctuations in the colour, intensity and saturation of each image, thus determining how severe the fluctuation of the flame is. The methodology was used for the full and the root flame region under different combustion scenarios across two experimental campaigns on a pilot-scale furnace.

The frequency spectrums constructed after the temperature oscillations were shown to be more spread, hence making it less sensitive to the presence of brighter particles that are characteristic of solid fuel combustion. Additionally, the frequency spectrums for the biomass were shown to be much sharper in comparison to the coal ones, with up to three discernible frequencies. A relevant frequency around 1 Hz was observed for the computed spectrums across all of the biomass combustion cases, which appears to be directly related to the fuel. In addition, the lack of relevant frequencies beyond 10 Hz suggests that those captured by the spectral analysis corresponds to the motion of bright particles in the flame region, rather than those associated with the volatile combustion phenomena.

The flame stability definition comprises a wide range of dynamic variables inherent to the combustion and fluid flow phenomena, complicating the convention on a singular approach in order to quantify it. After analysing the temporal repeatability and the magnitude of the flame parameter oscillations it can be concluded from the experimental results that, in general, the oxyfuel flames studied in this campaign appear to be more stable than their counterpart under air-fired conditions. In addition, the oscillation indices of the biomass combustion flames exhibited a narrower variation in comparison to the trends for coal combustion across the oxyfuel conditions, demonstrating that the flame stability appears to be less sensitive to the oxyfuel combustion environment for the biomass fuel in this study.

Acknowledgements

The authors would like to acknowledge the UK Carbon Capture and Storage Research Centre (UKCCSRC) and the SuperGEN Bioenergy Hub for their financial support of this research [Bio-CAP-UK: Air/Oxy Biomass Combustion with CO₂ Capture Technology, A UK Study; UKCCSRC-C1-40]. The PACT facilities form part of the UKCCSRC and are supported by BEIS and the EPSRC, through the RCUK Energy Programme; and to the Mexican Council for Science and Technology (CONACyT) for the scholarship granted.

References

- [1] International Energy Agency, "CO₂ Emissions From Fuel Combustion Highlights 2016," 2016.
- [2] WEC and W. E. Council, *World energy resources*. 2013.
- [3] BP, "BP Statistical Review of World Energy," British Petroleum, 2014.

- [4] IEA, "Technology roadmap, carbon capture and storage in industrial applications," International Energy Agency, 2011.
- [5] M. E. Boot-Handford, J. C. Abanades, E. J. Anthony, M. J. Blunt, S. Brandani, N. Mac Dowell, J. R. Fernández, M.-C. Ferrari, R. Gross, J. P. Hallett, R. S. Haszeldine, P. Heptonstall, A. Lyngfelt, Z. Makuch, E. Mangano, R. T. J. Porter, M. Pourkashanian, G. T. Rochelle, N. Shah, J. G. Yao, and P. S. Fennell, "Carbon capture and storage update," *Energy Environ. Sci.*, vol. 7, no. 1, pp. 130–189, Dec. 2014.
- [6] B. J. P. Buhre, L. K. Elliott, C. D. Sheng, R. P. Gupta, and T. F. Wall, "Oxy-fuel combustion technology for coal-fired power generation," *Prog. Energy Combust. Sci.*, vol. 31, no. 4, pp. 283–307, 2005.
- [7] T. Wall, Y. Liu, C. Spero, L. Elliott, S. Khare, R. Rathnam, F. Zeenathal, B. Moghtaderi, B. Buhre, C. Sheng, R. Gupta, T. Yamada, K. Makino, and J. Yu, "An overview on oxyfuel coal combustion—State of the art research and technology development," *Chem. Eng. Res. Des.*, vol. 87, no. 8, pp. 1003–1016, 2009.
- [8] M. B. Toftegaard, J. Brix, P. A. Jensen, P. Glarborg, and A. D. Jensen, "Oxy-fuel combustion of solid fuels," *Prog. Energy Combust. Sci.*, vol. 36, no. 5, pp. 581–625, 2010.
- [9] G. Scheffknecht, L. Al-Makhadmeh, U. Schnell, and J. Maier, "Oxy-fuel coal combustion—A review of the current state-of-the-art," *Int. J. Greenh. Gas Control*, vol. 5, pp. S16–S35, Jul. 2011.
- [10] Y. Huang, Y. Yan, G. Lu, and A. Reed, "On-line flicker measurement of gaseous flames by image processing and spectral analysis," *Meas. Sci. Technol.*, vol. 10, no. 8, pp. 726–733, Aug. 1999.
- [11] J. M. (János M. Beér and N. A. Chigier, *Combustion aerodynamics*. Applied Science Publishers Ltd, 1972.
- [12] A. K. Gupta, D. G. Lilley, and N. Syred, "Swirl flows," *Tunbridge Wells, Kent, England, Abacus Press. 1984, 488 p.*, 1984.
- [13] C. E. Baukal, R. (Robert E. . Schwartz, and John Zink Company., *The John Zink combustion handbook*. CRC Press, 2001.
- [14] G. Lu, G. Gilabert, and Y. Yan, "Vision based monitoring and characterisation of combustion flames," *J. Phys. Conf. Ser.*, vol. 15, no. 1, pp. 194–200, Jan. 2005.
- [15] P. Molcan, G. Lu, T. Le Bris, Y. Yan, B. Taupin, and S. Caillat, "Characterisation of biomass and coal co-firing on a 3MWth Combustion Test Facility using flame imaging and gas/ash sampling techniques," *Fuel*, vol. 88, no. 12, pp. 2328–2334, Dec. 2009.
- [16] L. G, Y. Y, and W. DD, "Advanced monitoring, characterisation and evaluation of gas-fired flames in a utility boiler," *J. Inst. Energy*, vol. 73, no. 494, pp. 43–49, 2000.
- [17] D. Sun, G. Lu, H. Zhou, and Y. Yan, "Flame stability monitoring and characterization through digital imaging and spectral analysis," *Meas. Sci. Technol.*, vol. 22, no. 11, p. 114007, Nov. 2011.
- [18] G. Lu, Y. Yan, M. Colechin, and R. Hill, "Monitoring of Oscillatory Characteristics of Pulverized Coal Flames Through Image Processing and Spectral Analysis," *IEEE Trans. Instrum. Meas.*, vol. 55, no. 1, pp. 226–231, Feb. 2006.

- [19] A. González-Cencerrado, B. Peña, and A. Gil, "Coal flame characterization by means of digital image processing in a semi-industrial scale PF swirl burner," *Appl. Energy*, vol. 94, pp. 375–384, Jun. 2012.
- [20] A. González-Cencerrado, A. Gil, and B. Peña, "Characterization of PF flames under different swirl conditions based on visualization systems," *Fuel*, vol. 113, pp. 798–809, 2013.
- [21] J. Smart, G. Lu, Y. Yan, and G. Riley, "Characterisation of an oxy-coal flame through digital imaging," *Combust. Flame*, vol. 157, no. 6, pp. 1132–1139, Jun. 2010.
- [22] N. Syred, "A review of oscillation mechanisms and the role of the precessing vortex core (PVC) in swirl combustion systems," *Prog. Energy Combust. Sci.*, vol. 32, no. 2, pp. 93–161, Jan. 2006.
- [23] P. Edge, S. R. Gubba, L. Ma, R. Porter, M. Pourkashanian, and A. Williams, "LES modelling of air and oxy-fuel pulverised coal combustion—impact on flame properties," *Proc. Combust. Inst.*, vol. 33, no. 2, pp. 2709–2716, Jan. 2011.
- [24] S. Black, J. Szuhánszki, L. Ma, D. B. Ingham, and M. Pourkashanian, "LES of a 250 kW oxy-coal burner: an investigation into flame stability," in *OCC3 Conference*, 2013.
- [25] M. Sami, K. Annamalai, and M. Wooldridge, "Co-firing of coal and biomass fuel blends," *Prog. Energy Combust. Sci.*, vol. 27, no. 2, pp. 171–214, Jan. 2001.
- [26] IEA, "IEA Energy Technology Essentials - Biomass for Power Generation and CHP," *High Temp.*, pp. 1–4, 2007.
- [27] S. G. Sahu, N. Chakraborty, and P. Sarkar, "Coal–biomass co-combustion: An overview," *Renew. Sustain. Energy Rev.*, vol. 39, pp. 575–586, Nov. 2014.
- [28] J. Kemper, "Biomass and carbon dioxide capture and storage: A review," *Int. J. Greenh. Gas Control*, vol. 40, pp. 401–430, Sep. 2015.
- [29] International Energy Agency, "Combining Bioenergy with CCS," 2011.
- [30] C. Gough and P. Upham, "Biomass energy with carbon capture and storage (BECCS or Bio-CCS)," *Greenh. Gases Sci. Technol.*, vol. 1, no. 4, pp. 324–334, Dec. 2011.
- [31] M. Fajardy and N. Mac Dowell, "Can BECCS deliver sustainable and resource efficient negative emissions?," *Energy Environ. Sci.*, vol. 10, no. 6, pp. 1389–1426, Jun. 2017.
- [32] G. Lu, Y. Yan, S. Cornwell, M. Whitehouse, and G. Riley, "Impact of co-firing coal and biomass on flame characteristics and stability," *Fuel*, vol. 87, no. 7, pp. 1133–1140, Jun. 2008.
- [33] A. González-Cencerrado, B. Peña, and A. Gil, "Experimental analysis of biomass co-firing flames in a pulverized fuel swirl burner using a CCD based visualization system," *Fuel Process. Technol.*, vol. 130, pp. 299–310, Feb. 2015.
- [34] A. Kotyra, W. Wójcik, K. Gromaszek, and G. Bazil, "Application of flame image series analysis in estimation of biomass and coal combustion operating point," *Przeglqd Elektrotechniczny*, no. R. 92, nr 8, pp. 129–132, 2016.
- [35] A. Kotyra, W. Wójcik, D. Sawicki, K. Gromaszek, A. Asembay, A. Sagymbekova, and A. Kozbakova, "Coal and biomass co-combustion process characterization using frequency analysis of flame flicker signals," in *Environmental Engineering V*, 2016, pp. 279–286.

- [36] J. Riaza, M. V. Gil, L. Álvarez, C. Pevida, J. J. Pis, and F. Rubiera, "Oxy-fuel combustion of coal and biomass blends," vol. 41, no. 1, pp. 429–435, 2012.
- [37] L. Álvarez, C. Yin, J. Riaza, C. Pevida, J. J. Pis, and F. Rubiera, "Oxy-coal combustion in an entrained flow reactor: Application of specific char and volatile combustion and radiation models for oxy-firing conditions," *Energy*, vol. 62, pp. 255–268, Dec. 2013.
- [38] L. Álvarez, C. Yin, J. Riaza, C. Pevida, J. J. Pis, and F. Rubiera, "Biomass co-firing under oxy-fuel conditions: A computational fluid dynamics modelling study and experimental validation," *Fuel Process. Technol.*, vol. 120, pp. 22–33, Apr. 2014.
- [39] J. Szuhánszki, S. Black, A. Pranzitelli, L. Ma, P. J. Stanger, D. B. Ingham, and M. Pourkashanian, "Evaluation of the Performance of a Power Plant Boiler Firing Coal, Biomass and a Blend Under Oxy-fuel Conditions as a CO₂ Capture Technique," *Energy Procedia*, vol. 37, pp. 1413–1422, Jan. 2013.
- [40] G. Lu, H. C. Bheemul, and Y. Yan, "Concurrent measurements of temperature and soot concentration of pulverised coal flames," in *IMTC 2001. Proceedings of the 18th IEEE Instrumentation and Measurement Technology Conference. Rediscovering Measurement in the Age of Informatics (Cat. No.01CH 37188)*, vol. 2, pp. 1221–1226.
- [41] D. Sun, G. Lu, H. Zhou, Y. Yan, and S. Liu, "Quantitative Assessment of Flame Stability Through Image Processing and Spectral Analysis," *IEEE Trans. Instrum. Meas.*, vol. 64, no. 12, pp. 3323–3333, Dec. 2015.
- [42] International Telecommunication Union, "Recommendation ITU-R BT.601-7, Studio encoding parameters of digital television for standard 4:3 and wide-screen 16:9 aspect ratios.," 2015.
- [43] R. D. Larrabee, "Spectral Emissivity of Tungsten†," *J. Opt. Soc. Am.*, vol. 49, no. 6, p. 619, Jun. 1959.
- [44] D. Sun, G. Lu, H. Zhou, and Y. Yan, "Flame stability monitoring and characterization through digital imaging and spectral analysis," *Meas. Sci. Technol.*, vol. 22, no. 11, p. 114007, Nov. 2011.
- [45] D. Sun, G. Lu, H. Zhou, X. Li, and Y. Yan, "A simple index based quantitative assessment of flame stability," in *2013 IEEE International Conference on Imaging Systems and Techniques (IST)*, 2013, pp. 190–193.
- [46] N. Otsu, "A Threshold Selection Method from Gray-Level Histograms," *IEEE Trans. Syst. Man. Cybern.*, vol. 9, no. 1, pp. 62–66, Jan. 1979.
- [47] I. W. Smith, "The combustion rates of coal chars: A review," *Symp. Combust.*, vol. 19, no. 1, pp. 1045–1065, Jan. 1982.